Acta Crystallographica Section D
Biological Crystallography
ISSN 0907-4449

Solving the structure of the bubble protein using the anomalous sulfur signal from single-crystal in-house Cu *Kα* diffraction data only

Johan Gotthardt Olsen,[a] Claus Flensburg,[b] Ole Olsen,[c] Gerard Bricogne[b] and Anette Henriksen[a]*

[a]Carlsberg Laboratory, Department of Chemistry, Gamle Carlsberg Vej 10, DK-2500 Valby, Denmark, [b]Global Phasing Ltd, Sheraton House, Castle Park, Cambridge CB3 0AX, England, and [c]Carlsberg Reseach Laboratory, Gamle Carlsberg Vej 10, DK-2500 Valby, Denmark

Correspondence e-mail: anette@crc.dk

Received 26 September 2003
Accepted 10 November 2003

PDB Reference: bubble protein, 1uoy, r1uoysf.

A small cysteine-rich protein, the function of which remains elusive, was discovered in the exudate of a *Penicillium* species. Crystal diffraction experiments conducted using in-house Cu *Kα* radiation and an R-AXIS IV++ imaging-plate detector yielded high-quality data to 1.4 Å, with a distinguishable anomalous signal from sulfur ($\Delta F/F = 0.031$). This was used to phase the data and solve the structure using a single data set; the 64-residue amino-acid sequence was unambiguously determined from the electron density. It revealed a globular all-β protein with a hitherto unknown fold, having a surface electrostatic charge distribution that is similar to that of another small secreted fungal protein, the *Williopsis mrakii* killer toxin. Aligning the charge distribution superimposed the potential recognition sites of the two proteins, suggesting a similar negatively charged target.

1. Introduction

Once crystals have been produced, phasing of diffraction data is the limiting step in the vast majority of cases in macromolecular crystallography. Recent publications have reported the use of the anomalous signal from sulfur in phase determination, either on its own or in combination with other techniques (Dauter *et al.*, 1999, 2002; Debreczeni *et al.*, 2003; Gordon *et al.*, 2001; Liu *et al.*, 2000; Micossi *et al.*, 2002). The anomalous contribution from sulfur, corresponding to 0.56 e^- at $\lambda = 1.54$ Å, is often too weak to yield a significant $\Delta F/F$ signal to allow structure determination by itself. The sulfur signal increases rapidly with decreasing radiation energy and tunable synchrotron radiation has been employed to improve signal-to-noise ratios. Dauter *et al.* (1999) used synchrotron radiation tuned to the Cu *Kα* wavelength in a test case using lysozyme to obtain sufficient anomalous signal to locate ten sulfurs and seven chloride ions with sufficient certainty to allow phasing of the data set; very recently, Debreczeni *et al.* (2003) traced the previously unknown structure of trypsin inhibitor from lima bean using Cu *Kα* radiation with a data redundancy of 85.

The fungus *Penicillium brevicompactum* Dierckx cultivated in our laboratory produces exudate droplets after 4–6 d of growth. HPLC, MS and SDS–PAGE analysis revealed the exudate to contain a number of secondary metabolites along with a 6.5 kDa hitherto unknown protein species denoted the bubble protein.

A number of fungi are known to secrete small cysteine-rich proteins that most likely exhibit different biological functions. Such proteins may be involved in hyphae coating and adherence (hydrophobins), plant invasion (elicitins) or defence (killer toxins). Within the latter two protein groups, however, there is a broad diversity with respect to molecular size,

structure and physical-chemical properties. The bubble protein in the present work is speculated to function as a killer toxin. Genes encoding killer toxins can be of viral, plasmid or nuclear origin, a diversity that is paralleled in an enormous heterogeneity of the translation products with respect to all structural levels. The *Ustilago maydis* killer toxin KP4 (Gu *et al.*, 1995) and the *Pichia farinosa* killer toxin SMK (Kashiwagi *et al.*, 1997) are both dimeric and share the same folding topology ($\alpha\beta$-sandwich) and presumably also the same target (inhibition of the Ca^{2+} channel). The KP6 killer toxin, also from *Ustilago maydis*, contains two polypeptide chains, of which the structure of the α-chain is known (Li *et al.*, 1999). This is also an $\alpha\beta$-sandwich but two right-handed $\beta\alpha\beta$ crossovers, in contrast to the left-handed crossovers of KP4 and SMK. KP6 is hypothesized to be a lethal membrane-pore-forming agent (Li *et al.*, 1999).

Two $\beta\gamma$-crystallin-fold killer toxins are known, the *Streptomyces* sp. killer toxin-like protein (Ohki *et al.*, 2001) and the *Williopsis mrakii* killer toxin (Antuch *et al.*, 1996). Although both proteins adopt the same fold, they exhibit different electrostatic properties, suggesting divergent evolution towards different targets. The bubble-protein structure reveals a novel protein fold/topology shared by no other published molecular structure. Despite this, the surface-charge distribution resembles that of the *W. mrakii* killer toxin, a property that suggests a case of convergent evolution: different fold, common molecular target.

2. Experimental

2.1. Protein source

P. brevicompactum Dierckx was inoculated in a Petri dish on solid agar containing 4.4 g MS medium, 1.0 g caseine hydrolysate, 3.5 g Phytagel and 30 g maltose per litre (all components from Sigma–Aldrich). Exudate droplets appeared after 4–6 d at 293 K and the exudate was harvested by 'skimming' the surface with a teaspoon after 7 d. The yield was 1–1.5 ml exudate per 12.5 cm diameter Petri dish. The harvest was filtered through a 0.22 mm cellulose acetate filter (Spin-X, Costar). Azide was added to a final concentration of 0.01%(*w*/*v*) and the extract was stored at 277 K.

2.2. Protein preparation, purification and crystallization

Exudate extract was loaded onto a cation-exchange column (Mono S 5/5 from Amersham Biosciences) in 30 m*M* sodium acetate buffer pH 5.0 and eluted with a linear gradient of 0–1 *M* NaCl in the same buffer over 30 column volumes. The major peak containing the bubble protein eluted at 300 m*M* NaCl. This fraction (4 ml) was then loaded onto a gel-filtration column (Amersham Biosciences HiPrep 16/60 Sephacryl S-100 HR) and eluted at 0.7 ml min^{-1} in 30 m*M* sodium acetate pH 5.0. The protein eluted after 87 ml in a single peak and proved to be pure based on visual inspection of an overloaded Coomassie-stained denaturing polyacrylamide gel (12% SDS–PAGE; Novagen System). The protein was concentrated (using Centriprep YM-30 and Microcon YM-30 centrifugal filter devices from Amicon) to 16 absorption units at 280 nm, corresponding to a theoretical concentration of 14 mg ml^{-1} or 2.1 m*M*. The protein was stored at 277 K and crystallized under these conditions. The largest dimension of the crystals was measured as 1 mm, but the crystal obtained by this method and used for the diffraction experiment measured 0.5 × 0.5 × 0.2 mm. The protein also crystallized in hanging drops consisting of 4 µl protein solution and 4 µl reservoir solution when equilibrated against a reservoir consisting of 17%(*w*/*v*) polyethylene glycol (PEG) 6000. The space group was found to be identical for the two conditions.

Table 1
Data-collection and model-building statistics.

Values in parentheses are for the outer shell (1.59–1.50 Å).

Data integration and scaling	
Space group	$C222_1$
No. of frames included	760
Unit-cell parameters (Å)	a = 43.6, b = 58.4, c = 53.4
Resolution (Å)	15.0–1.50
No. reflections	151997
No. unique reflections	11250
Completeness (%)	99.9 (99.9)
Anomalous completeness† (%)	99.9 (100.0)
Multiplicity	13.5
R_{anom}‡ (%)	1.6 (4.1)
R_{sym} (%)	
Overall	5.5
∞–4.74	4.3
4.74–3.35	3.9
3.35–2.74	4.3
2.74–2.37	5.5
2.37–2.12	5.5
2.12–1.94	6.9
1.94–1.79	7.8
1.79–1.68	9.2
1.68–1.58	12.5
1.58–1.50	15.5
$\langle I\rangle/\langle\sigma(I)\rangle$	8.3 (3.6)
$\Delta F/F$	0.031
Refinement	
No. molecules in asymmetric unit	1
MW (Da)	6640
Solvent content (%)	52
No. amino-acid residues/water molecules	64/129
R_{free}/R_{work} (%)	18.5/16.4
Average B values (Å^2)	
Main chain	10.3
Side chain	12.4
Water	29.8
Cross-validated estimated coordinate error§ (Å)	0.15
R.m.s.d. bond lengths (Å)	0.013
R.m.s.d. bond angles (°)	1.7

† Anomalous completeness covers the percentage of measured acentric reflections for which an anomalous difference was observed. ‡ $R_{anom} = \sum|\langle I^+\rangle - \langle I^-\rangle|/\sum(\langle I^+\rangle + \langle I^-\rangle)$. § The cross-validated estimated coordinate error is based on a Luzzati plot (Brünger *et al.*, 1998).

2.3. Data collection and processing

Crystals were transferred from the mother liquor to a 15%(*w*/*v*) PEG 6000 solution at 277 K and left in this solution for 1 min. The crystal was then subjected to 1 min incubations in 20, 30, 40 and 50% PEG 6000, respectively, followed by direct mounting of the crystal on the goniometer head in a

Table 2
Correlation between data redundancy, the number of correct sulfur sites located in *SHELXD* and the traceability of the resultant density-modified and solvent-flattened map.

No. of frames	Multiplicity	R_{sym}	No. of sites located in *SHELXD*	No. of residues traced by *ARP/wARP*
760	13.5	5.5	8	63
600	9.5	4.1	7	63
400	6.3	3.5	4	63
300	4.8	3.1	1	63
200	3.4	2.5	0	63†

† The solution from the 600-frame data set was taken as a starting point for the subsequent *SHARP* runs for the 200-frame data set.

stream of N_2 at 120 K. Although 35% PEG 6000 is a cryoprotectant solution, the diffraction pattern was slightly improved with respect to mosaicity by the high PEG 6000 concentration. Data were recorded on a Rigaku RU-H3RHB rotating Cu anode X-ray generator equipped with an R-AXIS IV++ imaging-plate detector and a 700-series Cryostream cooler from Oxford Cryosystems. An MSC/Confocal Max-Flux optical system in the blue configuration and with a 0.5 mm collimator was used to produced a focused monochromatic X-ray beam. The crystal-to-detector distance was set to 75 mm and a 380° data set was recorded with 0.5° oscillation around φ per frame. The exposure time was set to 150 s per frame after several initial attempts to determine crystal viability in the beam. The exposure time was chosen to obtain maximal exposure while ensuring the collection of a complete 360° data set from a single crystal without crystal deterioration. No attempt was made to measure Bijvoet pairs close in time. The diffraction pattern was indexed and integrated using *MOSFLM* (Leslie, 1999) and scaled using *SCALA* (Collaborative Computational Project, Number 4, 1994). Structure-factor amplitudes were calculated in *TRUNCATE* (French & Wilson, 1978). The crystals are orthorhombic, space group $C222_1$, with unit-cell parameters $a = 43.6$, $b = 58.4$, $c = 53.4$ Å. The dependence of the R_{sym} value on the data redundancy (Diederichs & Karplus, 1997) results in a relatively high R_{sym} value for the complete data set (5.5% for all 760 frames; Tables 1 and 2).

2.4. Phasing

The initial positions of the S atoms were found using *SHELXD* (Schneider & Sheldrick, 2002) in the 'look for disulfide' mode: a randomly oriented vector of length 2 Å is used to select peaks for the translation search, allowing the minimum interatomic distance to be 1.8 Å. Out of the 20 trials, 17 trials passed into crossword and PATFOM computation. An *autoSHARP* job was submitted for all 17 sets of coordinates and in most cases all eight sulfurs were correctly located. In the cases where one or more of the initial sites were incorrect, the residual maps calculated with *SHARP* clearly showed the remaining sites, except for one set of coordinates. After automatic solvent flattening, 16 trials had a correlation coefficient on E^2 of better than 0.70. The best *SHELXD* solution, with correlation coefficients of 20.69% for all and 5.96% for weak data, had four pairs of atoms with interatomic distances ranging from 2.1 to 2.3 Å. Only data to a resolution of 1.8 Å were used. The four pairs of atoms were then input to *SHARP* (Flensburg *et al.*, 2004; de La Fortelle & Bricogne, 1997; Vonrhein *et al.*, 2004) and optimized using all data. The overall figure of merit at the end of the *SHARP* run was 0.44. Inspection of the log-likelihood residual map indicated no missing features. The Fourier map was not easily traceable (Fig. 1*a*).

Determination of the correct hand, density modification and solvent flattening (*DM* and *SOLOMON*; Collaborative Computational Project, Number 4, 1994; Abrahams & Leslie, 1996) resulted in a fully traceable Fourier map (Fig. 1*b*). Initial model building (*ARP/wARP*; Perrakis *et al.*, 1999) and refinement (*REFMAC*; Murshudov *et al.*, 1997) were carried out automatically as implemented in the *autoSHARP* procedure (Vonrhein *et al.*, 2004). A single chain of 63 residues and 163 additional solvent molecules were detected, giving R and R_{free} values of 19.7 and 22.0%, respectively. A C-terminal cysteine residue involved in a disulfide bond was not built by the *ARP/wARP* procedure, although significant density was present. This residue was inserted by hand, giving a total of 64 residues in the model.

The structure could be traced using a minimum of 300 frames (150°), which was the number of frames needed to locate one S atom in *SHELXD*. Subsequent S atoms could then be located in an iterative *SHARP* procedure, in which residual map inspection was followed by heavy-atom-site optimization. If all sulfur sites were input to *SHARP*, only 200 frames were needed to produce an auto-traceable electron-density map (Table 2).

2.5. Refinement

The solvent molecules located by *ARP/wARP* were omitted from the structural refinement carried out using the program package *CNS* (Brünger *et al.*, 1998). Bulk-solvent correction and the 'anisotropic_fixed_isotropic' option for overall B-factor correction were applied throughout. The entire resolution range (1.5–15 Å) was included in the refinement. The polypeptide model was refined by a single round of annealing with virtually no effect on the R factors (R and R_{free} = 28.9 and 29.0%, respectively). Subsequently, 129 water molecules were included in the model using the automated water-picking procedure from *CNS*. The water molecules included corresponded to molecules initially build by *ARP/wARP*, but after the *CNS* algorithm had rejected 34 of them. Minor model adjustments were made using the graphics program *TURBO-FRODO* (Roussel & Cambillau, 1991). Positional refinement against X-ray data were performed on the adjusted model. Individual B-factor refinement on all atoms finalized the model. Statistics are shown in Table 1. Of all non-glycine residues, 91.8% are in the core regions of the Ramachandran plot and 8.2% are in the allowed regions (Laskowski *et al.*, 1993).

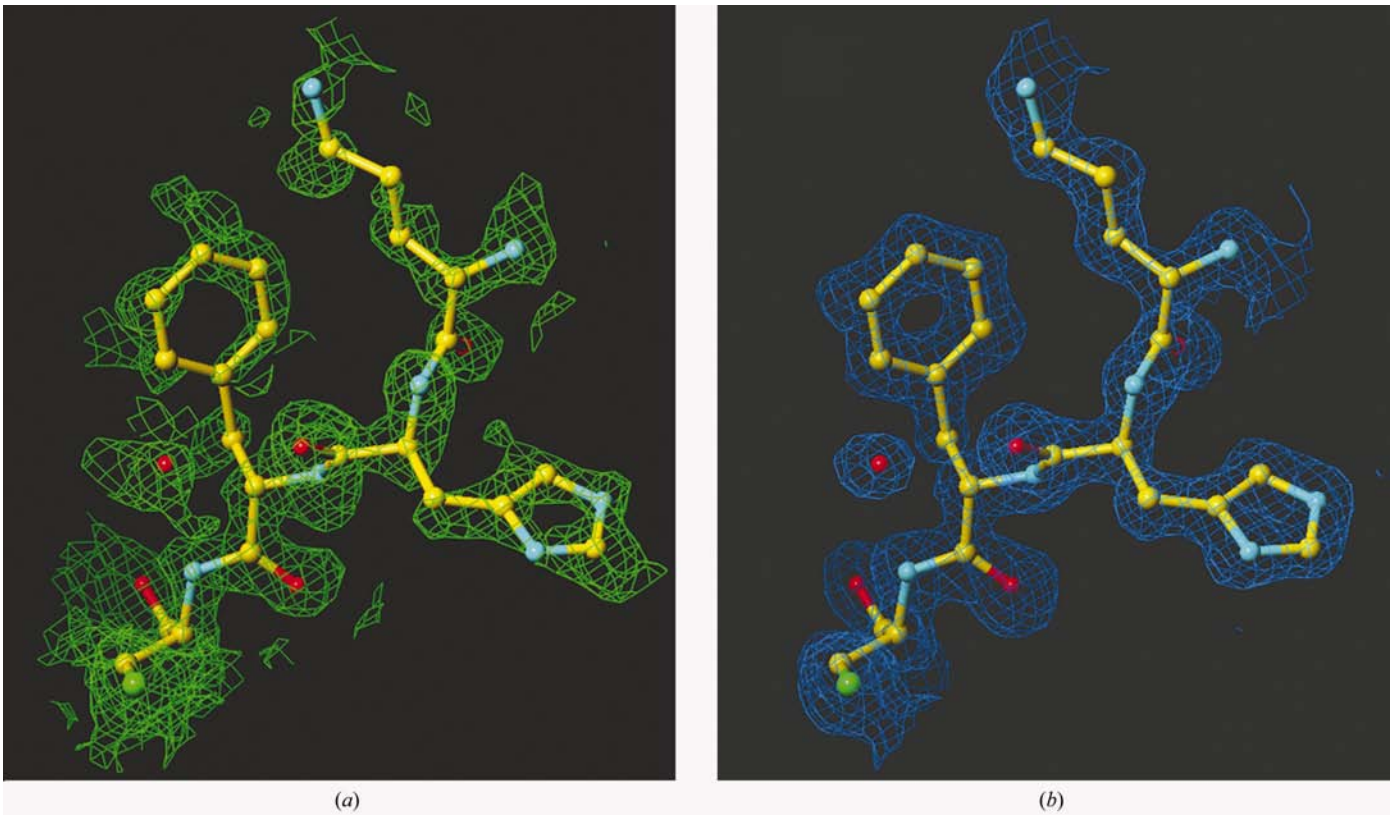

Figure 1
A representative area of the experimental SAD Fourier map at 1.2σ obtained from phases calculated in *SHARP* and structure factors from the data set comprising all 760 frames (*a*) before and (*b*) after density modification. The map is superimposed on the refined model. The figure was prepared in *TURBO-FRODO* (Roussel & Cambillau, 1991).

```
1          11         21         31         41         51         61
DTCGSGYNVD QRRTNSGCKA GNGDRHFCGC DRTGVVECKG GKWTEVQDCG SSSCKGTSNG GATC
```

Figure 2
Primary sequence of the mature bubble protein deduced from gene sequencing and corresponding to the sequence obtained by automated model building by *ARP*/*wARP*.

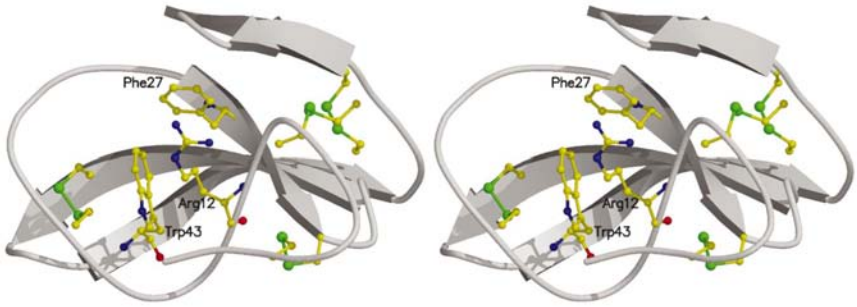

Figure 3
Ribbon representations of the bubble-protein fold. (*a*) Two disulfide bridges connect the extended structure to sheet 1 and another two cystines connect sheets 1 and 2. The cysteine residues are indicated, showing C^{α}, C^{β} and S^{γ} in ball-and-stick representation. The salt bridge between Asp10 and Arg32 is indicated. (*b*) The protein turned 65° counterclockwise around the vertical axis with respect to (*a*). The 64-amino-acid protein is composed of an N-terminal extended structure, a three-stranded β-sheet (sheet 1) and a C-terminal two-stranded β-sheet (sheet 2). This orientation focuses on the basic shallow funnel defined by the 26 C-terminal residues in extended configuration plus the type I tight turn between the two strands of sheet 2. The centre of the funnel contains Arg12, Phe27 and Trp43. This could be a potential recognition site for a negatively charged target (figure produced with *MOLSCRIPT*; Kraulis, 1991).

3. Structural analysis

The final model contains the entire polypeptide chain in addition to 129 water molecules. A total of 63 of the 64 amino-acid side chains were unambiguously docked into the electron density using the automated model-building procedure in *ARP*/*wARP* (Morris *et al.*, 2002). The sequence constructed by the *ARP*/*wARP* procedure corresponded to that deduced from gene sequencing (Fig. 2). All residues can be fitted to the map in one distinct conformation. Electron density is poorly defined for the side chain of Lys42.

3.1. Crystal packing

There is one polypeptide molecule per asymmetric unit. The interactions giving rise to the twofold axis along the *a* axis involve the hydrogen bonds between Lys55 N^{ζ} and Ser52 O^{γ} and between Asn8 N^{δ} and the backbone O atom of Gly6. The total buried interface along the *a* axis constitutes 624 Å^2 (calculated in *CNS*; Brünger *et al.*, 1998). The interactions along the *b* axis exclude

587 Å^2 from solvent exposure and are dominated by van der Waals interactions, except for a hydrogen bond between Gly21 O and Asp24 N, forming an irregular intermolecular β-sheet held together by two hydrogen bonds. On the interface along the *c* axis, Lys19 N$^{\zeta}$ makes four hydrogen bonds to the symmetry-related molecule (to Asp48 O$^{\delta1}$, Thr33 O$^{\gamma}$ and O and to Glu45 O$^{\varepsilon2}$). Asp48 O$^{\delta2}$ forms a hydrogen bond to the backbone N of Lys19. Furthermore, Asp1 O$^{\delta1}$ accepts a hydrogen bond from Asp48 N. A total of 436 Å^2 is buried at this interface.

3.2. Overall fold

The protein belongs to the all-β class (Fig. 3). The first 26 residues are in an extended conformation in the shape of a figure of eight (Fig. 3). A three-stranded meander β-sheet with a right-handed twist follows the extended structure (sheet 1, residues 27–49). The ten C-terminal residues (55–64) constitute a two-stranded sheet held together by four hydrogen bonds involving just two residue pairs. The protein contains four disulfide bonds, two of which connect the loop region to sheet 1 and the remaining two of which connect sheet 1 to the base of sheet 2. The two strands of sheet 2 are connected *via* a type I turn, which completes a mouth-like opening the shape of a shallow funnel together with the first 26 N-terminal residues. The accessible surface area of the funnel is 39 Å^2 and the volume enclosed amounts to 101 Å^3 (calculated using *CASTp*; Liang *et al.*, 1998). The funnel is the largest cavity found in the molecule, which may indicate that it is a feature relevant to the protein function (Laskowski *et al.*, 1996). No proteins of similar fold were detected by three-dimensional searches using *DALI* (Holm & Sander, 1993) or *DEJAVU* (Kleywegt & Jones, 1997).

The overall charge of the molecule at neutral pH is calculated to be +1.6 (*GRASP*; Nicholls *et al.*, 1991). The theoretical pI value is 7.7, which is 0.5 above the experimental value obtained by isoelectric focusing on polyacrylamide gel. An accessible-surface map representation of the electrostatic potential distribution calculated in *GRASP* shows that the protein has a heterogeneous and very distinct charge distribution (Fig. 4*a*). The acidic pole is dominated by hydroxyl-containing side chains (Thr33, Ser51, Ser52, Ser53 and Thr63) and acidic groups (Asp31, Glu45, Asp48 and the C-terminus). The funnel end is basic and dominated by basic amino-acid side chains (Arg12, Arg13, Arg25, Arg32, Lys39 and Lys42). A tryptophan (Trp43), a phenylalanine (Phe27) and an arginine (Arg12) sit at the base of the funnel.

3.3. Comparison to a killer toxin

The structures of several secreted yeast killer toxins have been described, but none of them resemble the bubble protein with respect to their overall fold. It is notable that the 88-residue $\beta\gamma$-crystallin-fold killer toxin from *W. mrakii* (WmKT) shares some global features with the bubble protein. The two proteins have a similar surface-charge distribution featuring a small negative patch at one 'end' of the molecule and a large positively charged mouth-like opening at the other end. Aligning the molecules according to charge distribution leads to a crude superposition of the largest cavities found in each protein (Fig. 4). The largest solvent-accessible opening in WmKT (32 Å^2) is the entrance to the largest cavity (101 Å^3). These measures are comparable to those obtained for the

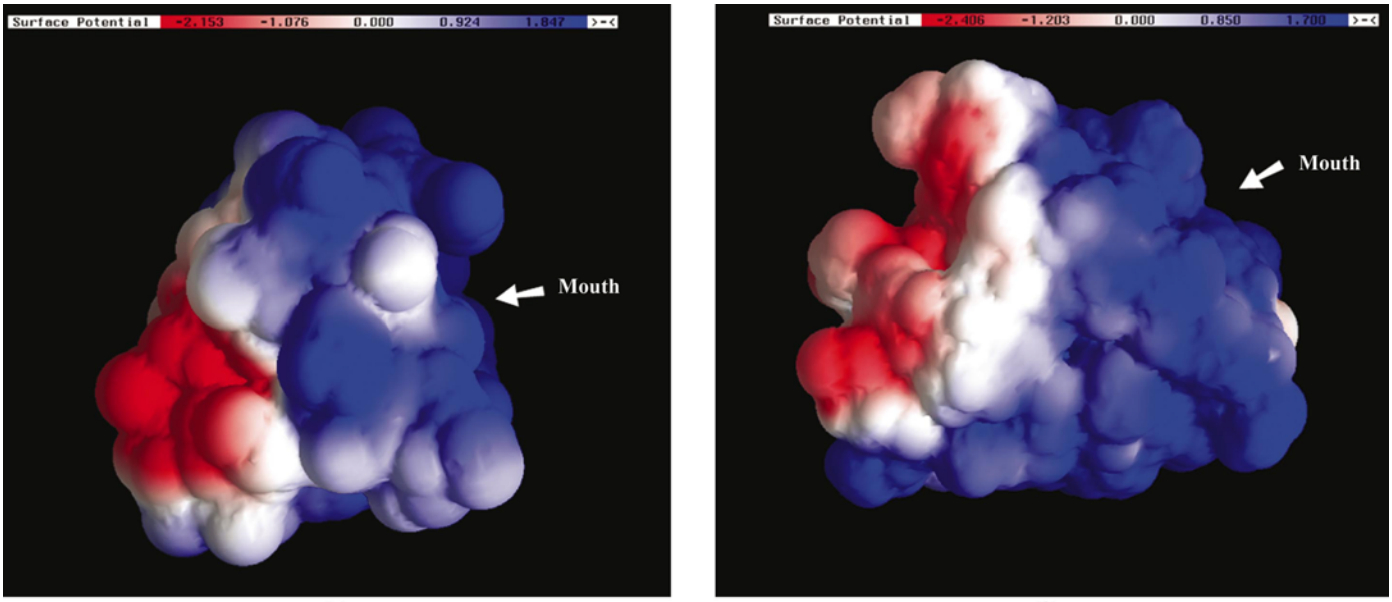

Figure 4
Accessible surface distribution of the electrostatic potential as calculated in *GRASP*. Blue indicates positive electrostatic potential and red negative. The molecule is bipolar, with a spectacular positively charged patch arising from a concentration of basic residues in the area around the funnel opening. (*a*) The bubble protein. (*b*) WmKT in the same relative orientation as the bubble protein in Fig. 2(*a*). The two proteins are aligned according to their electrostatic charge distribution.

bubble protein (a 39 Å^2 funnel opening to a 101 Å^3 cavity). It has been shown that in most cases the largest surface-accessible cavity in a protein corresponds to the ligand-binding site (Laskowski *et al.*, 1996). This could indicate a common molecular target and thus be an interesting example of convergent evolution.

The motif-recognition program *SPASM* (Kleywegt, 1999) was used to search for the Arg12, Phe27, Trp43 possible recognition site, but none of the hits [formaldehyde (and aldehyde) ferredoxin oxidoreductase and a maltodextrin phosphorylase] correspond to known binding sites and are therefore considered to be coincidental.

4. Conclusions

The present work shows that it is possible to phase protein diffraction data using the anomalous signal from sulfur recorded at Cu $K\alpha$ wavelength on laboratory equipment where the theoretical f'' contribution amounts to a mere 0.56 e$^-$. The electron-density modification step was essential to obtain an interpretable map.

The biological function of the bubble protein remains unknown. It is found in exudate droplets on the surface of *P. brevicompactum* Dierckx. Since it is the only protein detected in the exudate, it is tempting to suggest an antimicrobial or insecticidal role in line with the functions assigned to other small secreted fungal proteins. The structure of the 64-residue bubble protein reveals a hitherto unknown polypeptide fold composed of a 26-residue N-terminal stretch in extended conformation followed by a three-stranded β-sheet to which the N-terminal 'loop' is connected *via* two disulfide bridges. This sheet is followed by a second irregular two-stranded antiparallel β-sheet. The relative orientation of the two sheets is unusual and they make very little contact, in contrast to the usual sandwich and barrel motifs. Disulfide bridges and main-chain hydrogen bonds, with the exception of the Asp10–Arg32 salt bridge that connects to main-chain atoms of Cys54 and Gly56, ensure the relative positioning of the two sheets. Crystal-packing interactions are extensive and the existence of dimers and/or oligomers cannot be excluded. However, the largest buried surface area amounts to 624 Å^2, which is considered low even for a protein this size (Miller *et al.*, 1987).

The bipolar nature of the protein and the basic funnel suggests that the protein can recognize a molecule or part of a molecule with a negatively charged surface potential. This could be a structure on the surface of a competing or foraging organism.

The authors would like to thank Dr Jens Christian Frisvad of The Technical University of Denmark for identification of the *Penicillium* species.

References

Abrahams, J. P. & Leslie, A. G. W. (1996). *Acta Cryst.* D**52**, 30–42.
Antuch, W., Guntert, P. & Wuthrich, K. (1996). *Nature Struct. Biol.* **3**, 662–665.
Brünger, A. T., Adams, P. D., Clore, G. M., DeLano, W. L., Gros, P., Grosse-Kunstleve, R. W., Jiang, J.-S., Kuszewski, J., Nilges, M., Pannu, N. S., Read, R. J., Rice, L. M., Simonson, T. & Warren, G. L. (1998). *Acta Cryst.* D**54**, 905–921.
Collaborative Computational Project, Number 4 (1994). *Acta Cryst.* D**50**, 760–763.
Dauter, Z., Dauter, M., de La Fortelle, E., Bricogne, G. & Sheldrick, G. M. (1999). *J. Mol. Biol.* **289**, 83–92.
Dauter, Z., Dauter, M. & Dodson, E. (2002). *Acta Cryst.* D**58**, 494–506.
Debreczeni, J. É., Bunkoczi, G., Girmann, B. & Sheldrick, G. M. (2003). *Acta Cryst.* D**59**, 393–395.
Diederichs, K. & Karplus, P. A. (1997). *Nature Struct. Biol.* **4**, 269–275.
Flensburg, C., Paciorek, W., Schiltz, M., Vonrhein, C. & Bricogne, G. (2004). In preparation.
French, S. & Wilson, K. (1978). *Acta Cryst.* A**34**, 517–525.
Gordon, E. J., Leonard, G. A., McSweeney, S. & Zagalsky, P. F. (2001). *Acta Cryst.* D**57**, 1230–1237.
Gu, F., Khimani, A., Rane, S. G., Flurkey, W. H., Bozarth, R. F. & Smith, T. J. (1995). *Structure*, **3**, 805–814.
Holm, L. & Sander, C. (1993). *J. Mol. Biol.* **233**, 123–138.
Kashiwagi, T., Kunishima, N., Suzuki, C., Tsuchiya, F., Nikkuni, S., Arata, Y. & Morikawa, K. (1997). *Structure*, **5**, 81–94.
Kleywegt, G. J. (1999). *J. Mol. Biol.* **285**, 1887–1897.
Kleywegt, G. J. & Jones, T. A. (1997). *Methods Enzymol.* **277**, 525–545.
Kraulis, P. J. (1991). *J. Appl. Cryst.* **24**, 946–950.
La Fortelle, E. de & Bricogne, G. (1997). *Methods Enzymol.* **276**, 472–494.
Laskowski, R. A., Luscombe, N. M., Swindells, M. B. & Thornton, J. M. (1996). *Protein Sci.* **5**, 2438–2452.
Laskowski, R. A., MacArthur, M. W., Moss, D. S. & Thornton, J. M. (1993). *J. Appl. Cryst.* **26**, 283–291.
Leslie, A. (1999). *MOSFLM User's Guide.* MRC Laboratory of Molecular Biology, Cambridge, England.
Li, N., Erman, M., Pangborn, W., Duax, W. L., Park, C. M., Bruenn, J. & Ghosh, D. (1999). *J. Biol. Chem.* **274**, 20425–20431.
Liang, J., Edelsbrunner, H. & Woodward, C. (1998). *Protein Sci.* **7**, 1884–1897.
Liu, Z. J., Vysotski, E. S., Chen, C. J., Rose, J. P., Lee, J. & Wang, B.-C. (2000). *Protein Sci.* **9**, 2085–2093.
Micossi, E., Hunter, W. N. & Leonard, G. A. (2002). *Acta Cryst.* D**58**, 21–28.
Miller, S., Lesk, A. M., Janin, J. & Chothia, C. (1987). *Nature (London)*, **328**, 834–836.
Morris, R. J., Perrakis, A. & Lamzin, V. S. (2002). *Acta Cryst.* D**58**, 968–975.
Murshudov, G. N., Vagin, A. A. & Dodson, E. J. (1997). *Acta Cryst.* D**53**, 240–255.
Nicholls, A., Sharp, K. A. & Honig, B. (1991). *Proteins*, **11**, 281–296.
Ohki, S. Y., Kariya, E., Hiraga, K., Wakamiya, A., Isobe, T., Oda, K. & Kainosho, M. (2001). *J. Mol. Biol.* **305**, 109–120.
Perrakis, A., Morris, R. & Lamzin, V. S. (1999). *Nature Struct. Biol.* **6**, 458–463.
Roussel, A. & Cambillau, C. (1991). *Silicon Graphics Geometry Partners Directory*, p. 86. Mountain View, CA, USA: Silicon Graphics.
Schneider, T. R. & Sheldrick, G. M. (2002). *Acta Cryst.* D**58**, 1772–1779.
Vonrhein, C., Blanc, E., Roversi, P. & Bricogne, G. (2004). In preparation.

Acta Crystallographica Section D
Biological Crystallography
ISSN 0907-4449

addenda and errata

Solving the structure of the bubble protein using the anomalous sulfur signal from single-crystal in-house Cu *Kα* diffraction data only. Erratum

Johan Gotthardt Olsen,[a] Claus Flensburg,[b] Ole Olsen,[c] Marcus Seibold,[c] Gerard Bricogne[b] and Anette Henriksen[a]*

[a]Carlsberg Laboratory, Department of Chemistry, Gamle Carlsberg Vej 10, DK-2500 Valby, Denmark, [b]Global Phasing Ltd, Sheraton House, Castle Park, Cambridge CB3 0AX, England, and [c]Carlsberg Reseach Laboratory, Gamle Carlsberg Vej 10, DK-2500 Valby, Denmark. Correspondence e-mail: anette@crc.dk

In the paper by Olsen *et al.* [(2004), *Acta Cryst.* D**60**, 250–255] the author Marcus Seibold was inadvertently missed out. The correct list of authors is given above.

References

Olsen, J. C., Flensburg, C., Olsen, O., Bricogne, G. & Henriksen, A. (2004). *Acta Cryst.* D**60**, 250–255.

  DOI: 10.1107/S0907444904002598